DOI 10.1007/s11015-023-01604-2
Metallurgist, Vol. 67, Nos. 7-8, November, 2023 (Russian Original Nos. 7-8, July–August, 2023)

DEFORMATION BEHAVIOR, MICROSTRUCTURE AND MECHANICAL PROPERTIES OF NEW Al–Cu–Yb(Gd)–Mg–Mn–Zr ALLOYS

O. I. Mamzurina,[1] **S. M. Amer,**[2] **M. V. Glavatskikh,**[3]
R. Yu. Barkov,[4] **M. G. Khomutov,**[5] **and A. V. Pozdniakov**[6]

UDC 669.017

Deformation behavior, microstructure and mechanical properties of Al–Cu–Yb(Gd)–Mg–Mn–Zr alloy sheets are investigated. Based upon results of processing maps, optimum regimes for thermomechanical treatment at temperatures of 490–540°C and speeds of 0.01–1 sec^{-1} are determined. Annealing of cold-rolled sheets at temperatures up to 180°C leads to predominance of a strengthening effect due to aging over weakening from polygonization. Annealing of alloy sheets for 1 h at 400°C forms a partly recrystallized structure with a clear reduction in hardness from 145 HV to 75 HV. After 2 hours of annealing at 150°C, alloy combines a high yield strength of 412–417 MPa, a tensile strength of 441–449 MPa, and a good relative elongation of 2.7–3.2%. Sheet hardening followed by aging makes it possible to increase ductility by up to 5–8%, while the yield strength is 300–306 MPa with tensile strength of 364–389 MPa.

Keywords: aluminum alloys, ytterbium, gadolinium , microstructure, mechanical properties, dispersoids.

Introduction

Aluminum alloys play an important role in industry due to good specific strength, and technological efficiency during melting and forming. A study of alloy behavior during hot deformation is an important task during examination and development of new aluminum alloys [1–8]. Hot deformation facilitates an improvement in structure of ingots by reducing porosity, breaking down phases of crystallization origin with unfavorable morphology and grain structure refinement. As a result of this there is an increase in material strength and ductility.

Ternary quasibinary alloys Al–Cu–REM (where REM is rare earth metals Ce, Y, Er, Yb, Gd) with a Cu/REM atomic ratio equal to 4, having a narrow crystallization range, high solidus temperature and thermal stability for phase of crystallization origin, are promising for development of new materials based upon them [8–19]. By additional alloying with zirconium [20–23], manganese [24–26], magnesium [27–29] new heat-resistant high-tech cast and wrought alloys have been developed.

[1] National University of Science and Technology “MISIS”, Moscow, Russia; e-mail: mamzur309@mail.ru.
[2] [2]Al-Azhar University, Egypt, Cairo; e-mail: sayedeng_2010@yahoo.com.
[3] National University of Science and Technology “MISIS”, Moscow, Russia; e-mail: glavatskikh@edu.misis.ru.
[4] National University of Science and Technology “MISIS”, Moscow, Russia; e-mail: barkov@misis.ru.
[5] National University of Science and Technology “MISIS”, Moscow, Russia; e-mail: khomutov@misis.ru.
[6] National University of Science and Technology “MISIS”, Moscow, Russia; e-mail: pozdniakov@misis.ru.

Translated from Metallurg, Vol. 67, No. 8, pp. 48–56, August, 2023. Original article submitted February 10, 2023, revised article submitted February 24, 2023, original article accepted June 15, 2023.

Table 1
Test Alloy Chemical Composition, wt.%

Alloy designation	Al	Cu	Yb/Gd	Zr	Mn	Mg	Fe, Si, Ti
AlCuYbMg	Base	4.1	2.0	0.3	0.8	1.0	0.15 of each
AlCuGdMg	Base	4.5	2.7	0.3	0.8	1.1	

In order to develop the optimum alloy thermal deformation regime a study was made of its behavior during hot deformation. Normally in order to determine rheological properties there is use of thermal deformation stimulators [30, 31]. Dependences obtained in this way for "true-stress-strain" only make it possible to determine discrete regimes for limited selection of strain rates and temperature. Phenomenological modelling of alloy behavior during hot deformation is required in order to expand the temperature-rate ranges [32]. Models were plotted for alloys 2A14 [32], AA6099 [33], and AA6061 [34]. Also all studies in this direction have been conducted on classical wrought alloys with a matrix structure. However, it is well known that eutectic particles may have a marked effect on deformation behavior [35–39]. Eutectic particles are effective centers for generation of new recrystallized grains due to accumulation of dislocations within them during deformation treatment [36, 37]. This structure is exhibited by new cast heat-resistant alloys of the system Al–Cu–Yb(Gd)–Mg–Mn–Zr [29]. In this case, alongside alloys of similar composition and structure alloyed with yttrium or ytterbium [8, 28], new alloys of the system Al–Cu–Yb(Gd)–Mg–Mn–Zr are also promising deformable materials.

The aim of the present work is a study of the deformation behavior of new alloys during hot working under pressure and a study of the evolution of structure and properties of sheets of these alloys during post-deformation heat treatment.

Research Materials and Methods

The compositions of the test alloys AlCuYbMg and AlCuGdMg are provided in Table 1.

Alloys were melted in a resistance furnace from aluminum (99.7%), copper (99.5%), magnesium (99.5%) and master alloys Al–10Yb, Al–10Gd, Al–10Mn, Al–5Zr, Al–5Ti–1B at temperature 780–800°C. Master alloys Al–10Yb and Al–10Gd were melted from pure metals, although the most economic method is use of REM compounds. Ingots with a size of 20X40X100 m were prepared by casting into a copper water-cooled mold with a cooling rate of about 15°C/sec. Microstructural studies were conducted using a Zeiss optical microscope (OM), a TESCAN VEGA 3LMH scanning electron microscope (SEM) and a JEOL –2100 EX transmission electron microscope (TEM). Alloy specimen grain structure was studied in polarized light in an OM. Oxidation (15–25 V, 0–5°C) was performed in a Barker solution (46 mliter HBF_4, 7 g HBO_3 and 970 mliter H_2O). Specimens for TEM were prepared by electrolytic polishing in solution A2 in a Struers Tenupol-5 unit. Heat treatment was performed in Nabertherm and SNOL furnaces. Before rolling an ingots of alloys AlCuYbMg and AlCuGdMg they were homogenized at 555 and 565°C for 3 h followed by water quenching. Ingots were rolled in a longitudinal rolling mill duo-300 at 540°C from thickness of 20 mm to 10 mm and 1 mm (sheet) at room temperature. Rolling was accomplished with change in thickness for each pass by 0.5 mm in order to study evolution of the structure and properties after sheet rolling it was annealed at 150–550°C. Hardness was determined by the Vickers method with a load of 5 kg for 5–10 measurements. Tensile testing was conducted in a Zwick/Roell Z250 unit with a deformation rate of $3 \cdot 10^{-3}$ cm^{-1}.

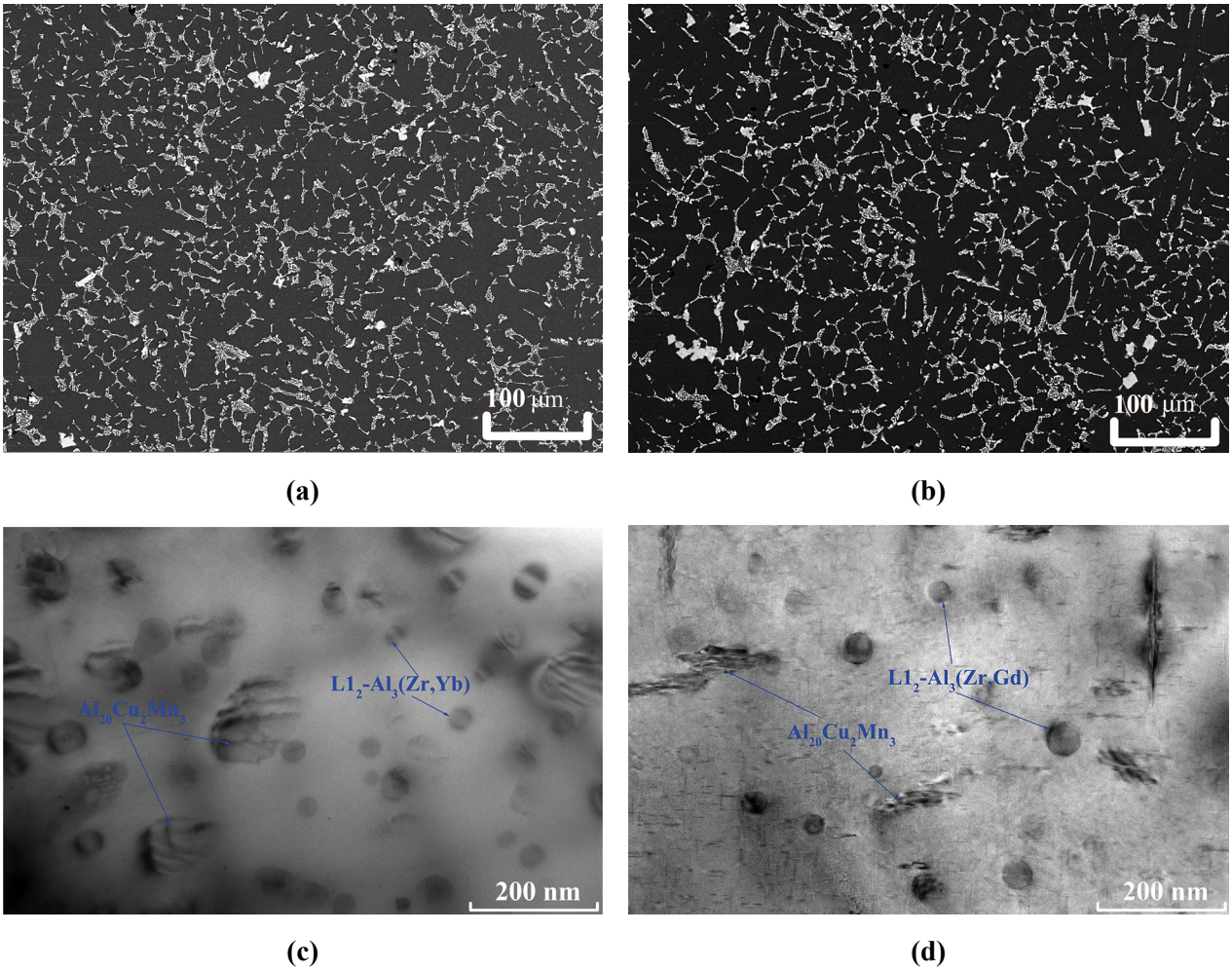

Fig. 1. Microstructure of alloys AlCuYbMg (a, c) and AlCuGdMg (b, d) after 3-h homogenization at 550 and 565°C respectively (SEM).

In order to model alloy deformation behavior compression testing was conducted using a Gleeble 3800 physical modelling complex thermomechanical process system on cylindrical specimens 10 mm in diameter and 15 mm thick. Compression was performed in the temperature range 390–540°C at a rate of 0.01–10 sec^{-1}. Specimens were heated to the test temperature at a rate of 5°C.sec, held for 30 sec, and cooled within an air stream at a rate of approximately 20°C/sec after testing. Compressive stress-deformation curves were processed taking account of friction and adiabatic warm-up during deformation [46, 47].

Results and Discussion

A detailed study of the cast microstructure and its evolution during homogenization have been provided in [29]. Provided in Fig. 1a, b is the structure of AlCuYbMg and AlCuGdMg after homogenization for 3 h at 550 and 565°C respectively. The structure is represented by aluminum solid solution and particles of phases $Al_{80-88}Cu_{8-12}Yb_{3-4}Mn$, $Al_{78-86}Cu_{10-15}Gd_{3-5}Mn$, $Al_{80}Yb_5Cu_6Si_8$, $Al_{80}Gd_5Cu_8Si_5$ of crystallization origin with sizes of the order of 1 μm (see Fig. 1a, b and [29]). In parallel with homogenization there was heterogenization, i.e., breakdown of the solution saturated with crystallization of zirconium, ytterbium or gadolinium

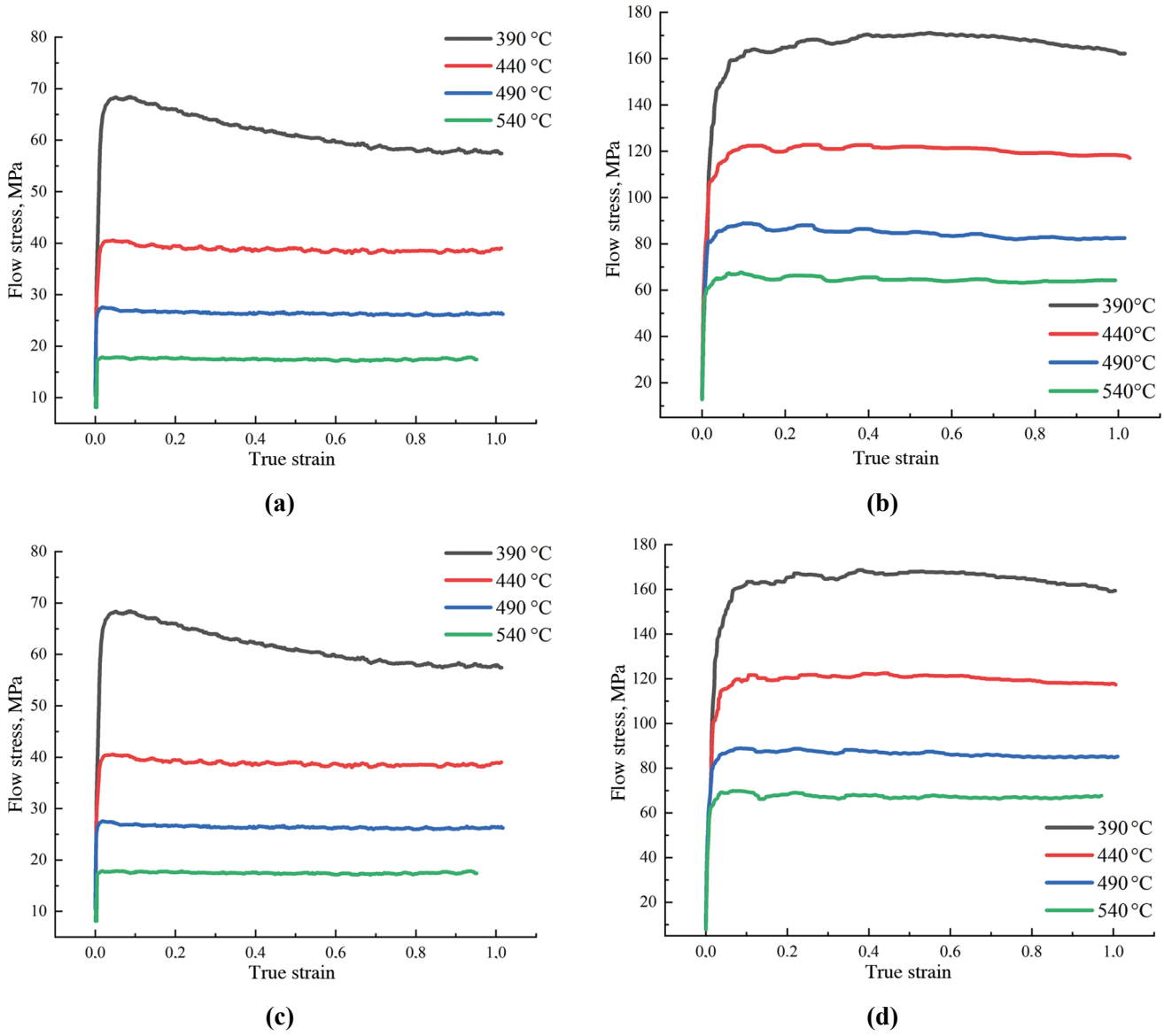

Fig. 2. Typical compression curves with rates 0.01 sec^{-1} (a, c) and 10 sec^{-1} (b, d) for alloys AlCuYbMg (a, b) and AlCuGdMg (c, d).

and manganese aluminum solid solution. As a result of heterogenization there is separation of dispersoids $Ll_2-Al_3(Zr, Yb)$ and $Ll_2-Al_3(Zr, Gd)$ with an average size of 28 ± 6 nm and 32 ± 4 nm respectively (see Fig. 1c, d in [29]), and also coarser particles of $Al_{20}Cu_3Mn_3$ with a size of 100–200 nm (see Fig. 1c, d in [29]). In this case experimental determination of the volume fraction of phases of crystallization origin in both alloys comprises 8%, calculated proportion of Ll_2-dispersoids – 0.7%, and phase $Al_{20}Cu_3Mn_3$–0.4–0.54% (see Fig. 1c, d, and [29]).

Typical compression curves are shown Fig. 2 for the alloys studied with rates of 0.01 and 10 sec^{-1}. Flow stress increases with an increase in deformation rate and with a reduction in temperature. With a rate of 0.01 sec^{-1} flow stresses are 18-70 MPa (see Fig. 2a, c), and with an increase in rate to 10 sec^{-1} stress increases to 60–160 MPa (see Fig. 2b, d). In this case a reduction in test temperature from 440 to 390°C leads to a sharp increase in stress (see Fig. 2a, c).

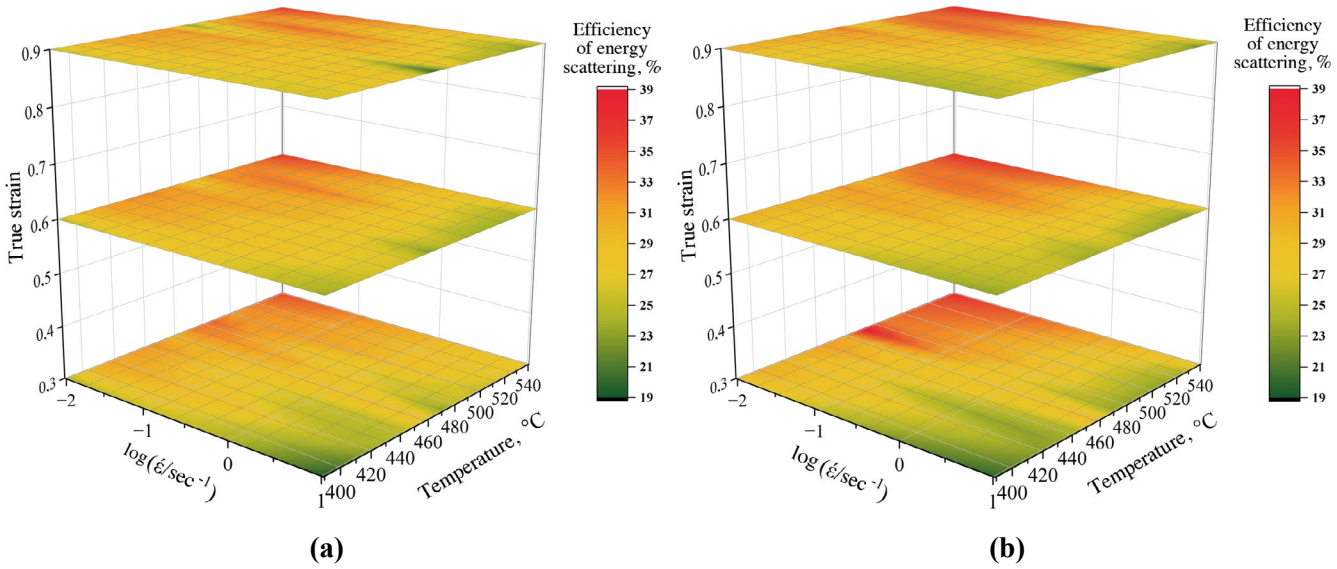

Fig. 3. Deformation 3D-maps for alloys AlCuYbMg (a) and AlCuGdMg (b).

Deformation maps are the main tool for selecting the optimum hot deformation regimes. Plotting a deformation map is based upon a material dynamic flow model [48]. During map construction effective energy dissipation is determined in relation to temperature and deformation rate. The efficiency of energy dissipation is determined by the material microstructure. Detailed plotting of a deformation map on the example of different aluminum alloys may be analyzed within works [8, 49–52]. Maps are provided in Fig. 3 for deformation of alloys AlCuYbMg and AlCuGdMg or the dependence of energy dissipation efficiency on temperature and deformation rate. Regions of the diagram with the maximum value of energy dissipation efficiency point to the optimum temperature-rate parameters for deformation. For both alloys this temperature range is 490–540°C and slow deformation rates.

Based upon the deformation maps plotted (see Fig. 3) ingots of alloys after 3 h of homogenization and quenching were rolled at 540°C from a thickness of 20 mm to 10 mm and to 1 mm of sheet at room temperature. The microstructure is provided in Fig. 4 for alloys AlCuYbMg and AlCuGdMg after rolling and the distribution of alloying elements between phases within a separate rectangle. Particles of crystallization origin phases are broken down and aligned in the rolling direction.

Dependences of alloy hardness on annealing time after rolling at low temperature are provided in Fig. 5a, c. Annealing after rolling stimulates the occurrence of two parallel processes. The first process of weakening is connected with recovery and polygonization, which slows down presence of dispersoids within the alloy structure. The second strengthening process is connected with ageing, which proceeds in view of forming supersaturated solid solution after hot rolling. As a result, at temperatures of 150 and 180°C in the first hours of annealing an increase in hardness is observed when ageing predominates over polygonization (see Fig. 5a, c) an increase in annealing time at 180°C and temperature to 210°C leads to prevalence of polygonization over ageing, as a result of which alloy hardness decreases and is stabilized (see Fig. 5a, c). Similar results have been obtained within alloys without magnesium and complex alloys of the Al–Cu–(Y, Er, Yb or Gd) systems [24–26, 28]. A further increase in annealing temperature to 350°C leads to a significant reduction in hardness, although in this case the structure remains unrecrystallized. Annealing for of both alloys at 400°C forms a partially recrystallized structure (see Fig. 5b, d). Within inserts of the microstructures partial recrystallization of the structure is seen: more than half of the recrystallized volume on a background of deformed fibers. The completeness of a recrystallized

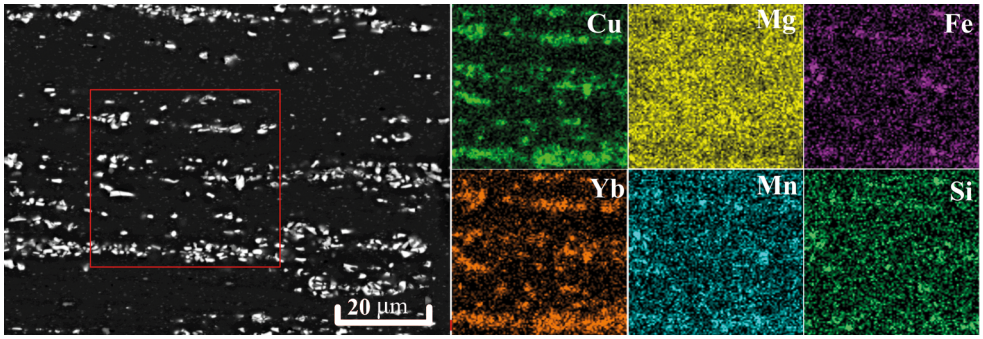

(a)

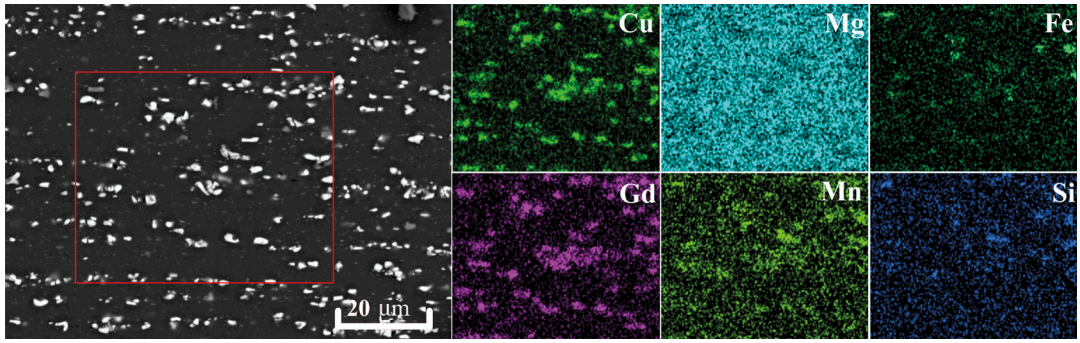

(b)

Fig. 4. Microstructure of alloys AlCuYbMg (a) and AlCuGdMg (b) after rolling (rolling direction over the horizontal) and alloying element distribution between phases within separate rectangle (SEM).

uniform structure with grain size of 6–8 is revealed after annealing at 450°C (see inserts in Fig. 5b, d). In this case in both alloys an increase in hardness is noted with an increase in annealing temperature from 400 to 450 and 550°C. In this case probably the increase in hardness is connected with natural ageing, proceeding after rapid sheet cooling in air. In addition, occurrence of breakdown of solid solution is possible with respect zirconium, ytterbium, or gadolinium, which initiate a high dislocation density, accumulated in the cold rolling stage. In this case there may be a sufficient stimulus for complete breakdown of the solid solution after casting. Similar results have been obtained in works [24–26, 28].

After rolling sheets alloys were quenched from the homogenizing temperature after holding for 15 min and aged at 150, 180, ad 210°C. Dependences for hardness on ageing time (Fig. 6) are qualitatively similar to those obtained with ageing of quenched ingots of these alloy [29]. Hardness increases during ageing from 81–89 *HV* to 125–128 *HV*. Strengthening in the ageing process is achieved due to separation of metastable S′(Al_2CuMg) phase as also during ageing of quenched ingots [29].

Annealing after rolling at 150°C did not reduce significantly the strength properties, increasing ductility (Table 2). After 2 h annealing at 150°C alloys are distinguished by a high yield strength of 412–417 MPa, ultimate strength 441–449 MPa, and low relative elongation 2.7–3.2%. For comparison wrought alloy D16 in a cold hardened and annealed conditions in the form of sheets [53] has a lower level of strength properties: yield strength 230–360 MPa, ultimate strength 365–475 MPa, but markedly greater relative elongation 8–13%, and in the form of bars [54] yield strength 325–345 MPa, ultimate strength 450–470 MPa, relative elongation 8–10%. A recrystallized structure created within alloys after annealing at homogenizing temperatures makes it possible to increase alloy ductility (see Table 2). According to tensile test results the relative elongation after

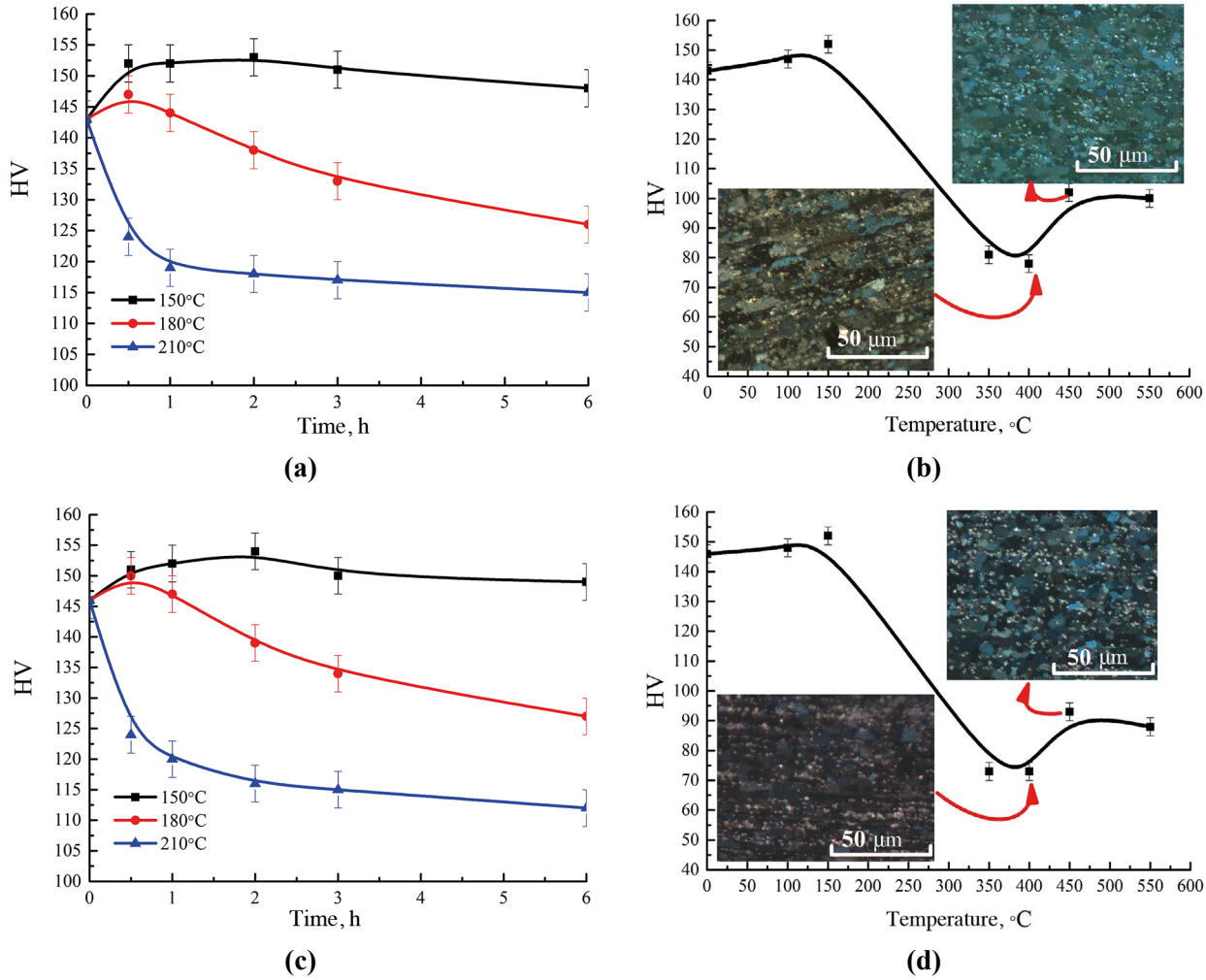

Fig. 5. Hardness evolution during annealing of sheets of alloys AlCuYbMg (a, b) and AlCuGdMg (c, d) [(a, c) are time dependences, (b, d) are temperature dependences after one hour annealing].

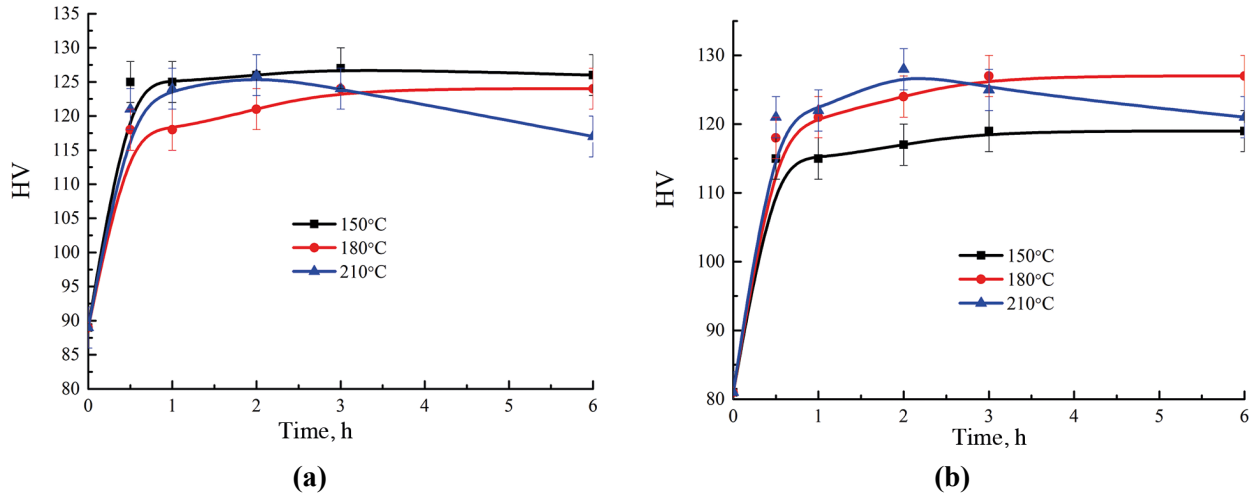

Fig. 6. Dependence of hardness on ageing time for alloys AlCuYbMg (a) and AlCuGdMg (b) after 15 min annealing at 500°C (a) and 565°C (b) of deformed sheets.

Table 2
Mechanical Property Characteristics after Rolling and Annealing

Condition	$\sigma_{0.2}$, MPa	σ_u, MPa	δ, %
Alloy AlCuYbMg			
Rolled	422 ± 2	425 ± 2	0.2 ± 0.1
Annealed 150°C, 2 h	417 ± 3	449 ± 1	2.7 ± 0.2
Annealed 210°C, 0.5 h	328 ± 3	352 ± 15	0.5 ± 0.3
Annealed 555°C, 0.25 h, quenching and ageing 210°C, 3 h	300 ± 7	364 ± 22	5.2 ± 2.0
Alloy AlCuGdMg			
Rolled	417 ± 3	438 ± 5	1.0 ± 0.8
Annealed 150°C, 2 h	412 ± 4	441 ± 2	3.2 ± 0.2
Annealed 210°C, 0.5 h	334 ± 2	368 ± 2	1.5 ± 0.1
Annealed 555°C, 0.25 h, quenching and ageing 210°C, 3 h	306 ± 1	389 ± 1	8.0 ± 2.4

ageing at 210°C for 3 h is 5–8% (see Table 2). In this case yield strength is 300–306 MPa, and ultimate strength is 356–365 MPa. Recrystallized bars of alloy D16 [54] are surpassed with respect to strength: yield point 265 MPa, ultimate strength 410 MPa, and relative elongation 12%. In this case the technological efficiency during casting alloy D16 is markedly lower than for the compositions studied. As a result, is may be concluded that the new wrought alloys based upon Al–Cu–Yb and Al–Cu–Gd systems may be competitive with existing industrial alloys.

CONCLUSIONS

The deformation behavior, microstructure and mechanical properties have been studied for sheets Al–Cu–Yb(Gd)–Mg–Mn–Zr by plotting deformation maps for testing in compression, light, scanning, and transmission electron microscopy, hardness measurement, and determination of physical property characteristics in tension. According to results of plotting deformation maps optimum thermal deformation treatment regimes have been determined at 490–540°C and rates of 0.01–1 sec^{-1}. A structure consisting of intermetallics of crystallization origin with a size of about 1 μm and dispersoids $L1_2-Al_3(Zr, Yb)$ and $L1_2-Al_3(Zr, Gd)$ with an average size of 28 ± 6 nm and 32 ± 4 nm and Al20Cu2Mn3 with a size of 100-200 nm makes it possible to achieve a high level of mechanical property characteristics. Low-temperature annealing at up 180°C for cold-rolled sheets leads to an increase in hardness, connected with prevalence of ageing over polygonization. Annealing for 1 h of both alloys at 400°C forms a partly recrystallized structure with a sharp reduction in hardness from 145 *HV* to 75 *HV*. After annealing for 2 h at 150°C in alloys there is a combination of high yield strength 412-417 MPa,

and ultimate strength 441–449 MPa, with low relative elongation of 2.7–3.2%. Quenching sheets followed by ageing makes it possible to increase ductility to 5–8%, yield strength in this case is 300–360 MPa, and the ultimate strength of 364–389 MPa.

Research was carried out due to a grant of the Russian Scientific Fund No. 21-79-00193, https://rscf.ru/project/21-79-00193/.

REFERENCES

1. P. Snopinski, M. Król, T. Tański, D. Pakuła, and A. Kříž, "Effect of initial microstructure on hot deformation behavior of AlMg5Si2Mn alloy," *Materials Characterization,* **177**, 111167 (2021).
2. C. Xu, H. He, Z. Xue, and L. Li, "A detailed investigation on the grain structure evolution of AA7005 aluminum alloy during hot deformation," *Materials Characterization,* **171**, 110801 (2021),
3. O. Bembalge and S. Panigrahi, "Hot deformation behaviour and processing map development of cryorolled AA6063 alloy under compression and tension," *Intern. J. Mechanical Sci.,* **191**, 106100 (2021).
4. J. Miao, S. Sutton, and A. A. Luo, "Microstructure and hot deformation behavior of a new aluminum–lithium–copper based AA2070 alloy," *Mater. Sci. Eng.: A,* **777**, 139048 (2020).
5. H. Wu, S. Wen, H. Huang, K. Gao, X. Wu, W. Wang, and Z. Nie, "Hot deformation behavior and processing map of a new type Al–Zn–Mg–Er–Zr alloy," *J. Alloys Compounds,* **685**, 869–880 (2016).
6. E. Scharifi, U. Savaci, Z. Kavaklioglu, U. Weidig, S. Turan, and K. Steinhoff, "Effect of thermo-mechanical processing on quench induced precipitates morphology and mechanical properties in high strength AA7075 aluminum alloy," *Materials Characterization,* **17**, 111026 (2021).
7. Y. Jiang, H. Ding, M. Cai, Y. Chen ,Y. Liu , and Y. Zhang, "Investigation into the hot forming-quenching integrated process with cold dies for high strength aluminum alloy," *Materials Characterization,* **158**, 109967 (2019).
8. M. G. Khomutov, S. M. Amer, R. Y. Barkov, M. V. Glavatskikh, A. Y. Churyumov, and A. V. Pozdniakov," Hot deformation behavior of novel Al-Cu-Y(Er)-Mg-Mn-Zr alloys," *Metals,* **1**, 1521 (2021).
9. T. Krachan, B. Stel'makhovych, and Y. Kuz'ma, "The Y-Cu-Al system," *J. Alloys Compounds,* **349**, 134–139 (2003).
10. L. Zhang, P. J. Masset, X. Tao, G. Huang, H. Luo, L. Liu, and Z. Jin, "Thermodynamic description of the Al–Cu–Y ternary system," *Calphad Comput. Coupling Phase Diagrams Thermochem.,* **35**, 574–579.
11. L. G. Zhang, L. B. Liu, G. H. Huang, H. Y. Qi, B. R. Jia, and Z. P. Jin, "Thermodynamic assessment of the Al–Cu–Er system," *Calphad Comput. Coupling Phase Diagrams Thermochem.,* **32**, 527–534 (2008).
12. L. Zhang, P. J. Masset, F. Cao, F. Meng, L. Liu, and Z. Jin, "Phase relationships in the Al-rich region of the Al–Cu–Er system," *J. Alloys Compounds,* **509**, 3822–3831 (2011).
13. G. Huang, L. Liu, L. Zhang, and Z. Jin, "Thermodynamic description of the Al–Cu–Yb ternary system supported by first principles calculations," *J. Mining and Metallurgy, Section B: Metallurgy,* **52**, 177–183 (2016).
14. N. A. Belov, A. V.,Khvan, and A. N. Alabin, "Microstructure and phase composition of Al–Ce–Cu alloys in the Al-rich corner," *Proc. Materials Sci. Forum,* **519–521**, 395–400 (2006).
15. N. A. Belov and A. V. Khvan, "The ternary Al–Ce–Cu phase diagram in the aluminum-rich corner," *Acta Materialia,* **55**, 5473–5482 (2007).
16. A. V. Pozdniakov and R. Y. Barkov, "Microstructure and materials characterisation of the novel Al–Cu–Y alloy," *Mater. Sci. and Techn. (UK),* **34**, 1489–1496 (2018).
17. A. V. Pozdnyakov, R. Y. Barkov, Z. Sarsenbaev, S. M. Amer, and A. S. Prosviryakov, "Evolution of microstructure and mechanical properties of a new Al–Cu–Er wrought alloy," *Physics Metals and Metallography,* **120**, 614–619 (2019).
18. S. M. Amer, R. Y. Barkov, O. A. Yakovtseva, and A. V. Pozdniakov, "Comparative analysis of structure and properties of quasibinary Al–6.5Cu–2.3Y and Al–6Cu–4.05Er alloys," *Physics Metals and Metallography,* **121**, 476–482 (2020).
19. S. M. Amer, R. Y. Barkov, and A. V. Pozdniakov, "Microstructure and mechanical properties of novel quasibinary Al–Cu–Yb and Al–Cu–Gd alloys," *Metals (Basel),* **11**, 1–11 (2021).
20. S. M. Amer, R. Yu. Barkov, O. A. Yakovtseva, I. S. Loginova, and A. V. Pozdniakov, "Effect of Zr on microstructure and mechanical properties of the Al–Cu–Er alloy," *Mater. Sci. Techn.,* **36**, 453–459 (2020).
21. A. V. Pozdniakov, R. Yu. Barkov, S. M. Amer, V. S. Levchenko, A. D. Kotov, and A. V. Mikhaylovskaya, "Microstructure, mechanical properties and superplasticity of the Al–Cu–Y–Zr alloy," *Mater. Sci. Eng.: A,* **758**, 28–35 (2019).
22. S. M. Amer, A. V. Mikhaylovskaya, R. Yu. Barkov, A. D. Kotov, A. G. Mochugovskiy O. A. Yakovtseva, M. V. Glavatskikh, I. S. Loginova, S. V. Medvedeva, and A. V. Pozdniakov, "Effect of homogenization treatment regime on microstructure, recrystallization behavior, mechanical properties, and superplasticity of Al–Cu–Er–Zr alloy," *JOM,* **73**, 3092–3101 (2021).

23. O. I. Mamzurina, S. M. Amer, I. S. Loginova, M. V. Glavatskikh, A. G. Mochugovskiy, R. Yu. Barkov, and A. V. Pozdniakov, "Effect of Zr on microstructure and mechanical properties of the Al–Cu–Yb and Al–Cu–Gd alloys," *Metals (Basel),* **12**, 479 (2022).
24. S. M. Amer, O. A. Yakovtseva, I. S. Loginova, S. V. Medvedeva, A. S. Prosviryakov, A. I. Bazlov, R. Yu. Barkov, and A. V. Pozdniakov, "The phase composition and mechanical properties of the novel precipitation-strengthening Al–Cu–Er–Mn–Zr alloy," *Applied Sciences-Basel,* **10(15)**, 5345 (2020).
25. S. M. Amer, R. Yu. Barkov, and A. V. Pozdniakov, "Effect of Mn on the phase composition and properties of Al–Cu–Y–Zr Alloy," *Physics Metals and Metallography,* **121**, No. 12, 1227–1232 (2020).
26. S. M., Amer, O. I. Mamzurina, I. S. Loginova, M. V. Glavatskikh, R. Yu. Barkov, and A. V. Pozdniakov, "Effect of Mn addition on the phase composition and strengthening behavior of AlCuYbZr and AlCuGdZr alloys," *JOM,* **74**, No. 9, 3646–3654 (2022).
27. S. M. Amer, R. Yu. Barkov, A. S. Prosviryakov, and A. V. Pozdniakov, "Structure and properties of new heat-resistant cast alloys based on the Al–Cu–Y and Al–Cu–Er systems," *Physics Metals and Metallography,* **122**, 908–914 (2021).
28. S. M. Amer, R. Yu. Barkov, A. S. Prosviryakov, and A. V. Pozdniakov, "Structure and properties of new wrought Al–Cu–Y- and Al–Cu–Er-based alloys," *Physics Metals and Metallography, B,* 915–922 (2021).
29. O. I. Mamzurina, S. M. Amer, M. V. Glavatskikh, R. Yu. Barkov, I. S. Loginova, and A. V. Pozdniakov, "Microstructure and mechanical properties of novel heat resistant cast Al–Cu–Yb(Gd)–Mg–Mn–Zr alloys," *Metals (Basel),* **12**, 2079 (2022).
30. M. G. Khomutov, A. I. Bazlov, A. A. Tsar'kov, and A. Yu. Churyumov, "Simulation of flow stress of single-phase aluminium alloys of the Al–Mg, Al–Cu and Al–Zn systems in the process of hot deformation," *Metal Science and Heat Treatment,* **55**, 393–396 (2013).
31. G. Krallics, Z. Bézi, and P. Bereczki, "Hot deformation properties of 8006 aluminium alloy," in: *Procedia Manufacturing,* Vol. 37 (2019), pp. 174–181.
32. Q. Wang, X. He, Y. Deng, J. Zhao, and X. Guo, "Experimental study of grain structures evolution and constitutive model of isothermal deformed 2A14 aluminum alloy," *J. Materials Research and Technology,* **12**, 2348–2367 (2021).
33. H. Hallberg, A. Chamanfar, and N. E. Nanninga, "A constitutive model for the flow stress behavior and microstructure evolution in aluminum alloys under hot working conditions—with application to AA6099," *Applied Mathematical Modelling,* **81**, 253–262 (2019).
34. A. Rudnytskyj, P. Simon, M. Jech, and C. Gachot, "Constitutive modelling of the 6061 aluminium alloy under hot rolling conditions and large strain ranges," *Material Design,* **190**, 108568 (2020).
35. A. Yu. Churyumov, A. Mikhaylovskaya, A. I. Bazlov, A. A. Tsarkov, A. D. Kotov, and S. A. Aksenov, "Influence of Al_3Ni crystallization origin particles on hot deformation behaviour of aluminium based alloys," *Philosophical Magazine,* **97**, 572–590 (2017).
36. Y. Wu, C. Liu, H. Liao, J. Jiang, and A. Ma, "Joint effect of micro-sized Si particles and nano-sized dispersoids on the flow behavior and dynamic recrystallization of near-eutectic Al–Si based alloys during hot compression," *J. Alloys and Compounds,* **856**. 158072 (2021).
37. A. Mikhaylovskaya, M. Ghayoumabadi, and A. Mochugovskiy, "Superplasticity and mechanical properties of Al–Mg–Si alloy doped with eutectic-forming Ni and Fe, and dispersoid forming Sc and Zr elements," *Mater. Sci. Eng.: A,* **817**, 141319 (2021).
38. Z. Zhang, J. Hu, J. Teng, J. Chen, G. Zhao, F. Jiang, D. Fu, and H. Zhang, "Hot compression and industrial extrusion characteristics of an as-cast Al–10Sr master alloy," *J. Manufacturing Processes,* **61**, 481–491 (2021).
39. S. Chankitmunkong, D. G. Eskin, and C. Limmaneevichitr, "Constitutive behavior of an AA4032 piston alloy with Cu and Er additions upon high-temperature compressive deformation," *Metal. Mater. Trans. A,* **51**, 467–481 (2019).
40. Y. I. Kosov and V. Y. Bazhin, "Synthesis of an aluminum–erbium master alloy from chloride–fluoride melts," *Russian Metallurgy (Metally),* **2**, 139–148 (2018).
41. S. Savchenkov, Y. Kosov, V. Bazhin, K. Krylov, and R. Kawalla, "Microstructural master alloys features of aluminum–erbium system," *Crystals,* **11**, No. 11, 1353 (2021).
42. Y. I. Kosov and V. Yu. Bazhin, "Features of phase formation during aluminothermal preparation of aluminum-erbium master alloy," *Metallurgist,* **62**, No. 5-6, 440–448 (2018).
43. Y. I. Kosov and V. Yu. Bazhin, and V. G. Povarov, "Interaction of erbium fluoride with alkali metal chloride–fluoride melts in synthesizing an Al–Er master alloy," *Russian Metallurgy(Metally),* **6**, 539–544 (2018).
44. Y. I. Kosov and V. Yu. Bazhin, "Preparation of novel Al–Er master alloys in chloride-fluoride melt," *Mater. Sci. Forum,* **918**, 21–27 (2018).
45. V. Yu. Bazhin, S. A. Savchenkov, and N.A. Gordevnin, "Investigation of the ytterbium reduction process in the synthesis of Al–Yb master alloys for the modification of aluminum alloys," *Non-Ferrous Metals,* **53**, No. 2, 65–72 (2022).
46. Z. Wan, L. Hu, Y. Sun, T. Wang, and Z. Li, "Hot deformation behavior and processing workability of a Ni-based alloy," *J. Alloys and Compounds,* **769**, 367–375 (2018).
47. A. Yu. Churyumov, M. G. Khomutov, A. A. Tsar'kov, A. V. Pozdnyakov, A. N. Solonin, V. M. Efimov, and E. L. Mukhanov, "Study of the structure and mechanical properties of corrosion resistant steel with a high concentration of boron at elevated temperatures," *Physics Metals and Metallography,* **115**, 809–813 (2014).
48. Y. V. R. K. Prasad, H. L. Gegel, S. M. Doraivelu, J. C. Malas, J. T. Morgan, K. A. Lark, and D. R. Barker, "Modeling of dynamic material behavior in hot deformation: Forging of Ti-6242," *Met. Trans. A,* **15**, 1883–1892 (1984).

49. M. G. Khomutov, A. V. Pozdniakov, A. Yu. Churyumov, A. N. Solonin, M. V. Glavatskikh, and R. Yu. Barkov, "Flow stress modelling and 3D processing maps of scandium contents," *Applied Sci.,* **11**. 4587 (2021).
50. B. Ke, L. Ye, J. Tang, Y. Zhang, S. Liu, H. Lin, Y. Dong, and X. Liu, "Hot deformation behavior and 3D processing maps of AA7020 aluminum alloy," *J. Alloys and Compounds,* **845**, 156113 (2020).
51. Y. Sun, Z. Cao, Z. Wan, L. Hu, W. Ye, N. Li, and C. Fan, "3D processing map and hot deformation behavior of 6A02 aluminum alloy," *J. Alloys and Compounds,* **742**, 356–368 (2018).
52. R. Wu, Y. Liu, C. Geng, Q. Lin, Y. Xiao, J. Xu, and W. Kang, "Study on hot deformation behavior and intrinsic workability of 6063 aluminum alloys using 3D processing map," *J. Alloys and Compounds,* **713**, 212–221 (2017).
53. *GOST 21631–76. Aluminum Sheets and Aluminium Alloys, Technical Specifications* [in Russian], Standartinform, Moscow (2008).
54. *GOST P-51834–2001. Bars, Extruded from Aluminium Alloys with High Strength and Increased Ductility. Technical Specifications* [in Russian], IPK Izd. Standartov, Moscow (2002).